Title

Mislocalization of cone nuclei impairs cone function in mice.

Journal

The FASEB Journal, 34(8)

Authors

Xue, Yunlu

Razafsky, David

Hodzic, Didier

et al.

Publication Date

2020-08-01

DOI

10.1096/fj.202000568R

Peer reviewed

HHS Public Access

Author manuscript

FASEB J. Author manuscript; available in PMC 2021 August 01.

Published in final edited form as:

FASEB J. 2020 August ; 34(8): 10242–10249. doi:10.1096/fj.202000568R.

Mislocalization of cone nuclei impairs cone function in mice

Yunlu Xue[1,2], **David Razafsky**[3], **Didier Hodizc**[3], **Vladimir J. Kefalov**[3]

[1]Department of Genetics, Harvard Medical School, Boston, MA 02115;

[2]Department of Ophthalmology, Harvard Medical School, Boston, MA 02115;

[3]Department of Ophthalmology & Visual Sciences, Washington University School of Medicine, St. Louis, Missouri 63110, USA

Abstract

The nuclei of cone photoreceptors are located on the apical side of the outer nuclear layer (ONL) in vertebrate retinas. However, the functional role of this evolutionarily conserved localization of cone nuclei is unknown. We previously showed that Linkers of the Nucleoskeleton to the Cytoskeleton (LINC complexes) are essential for the apical migration of cone nuclei during development. Here, we developed an efficient genetic strategy to disrupt cone LINC complexes in mice. Experiments with animals from both sexes revealed that disrupting cone LINC complexes resulted in mislocalization of cone nuclei to the basal side of ONL in mouse retina. This, in turn, disrupted cone pedicle morphology, and appeared to reduce the efficiency of synaptic transmission from cones to bipolar cells. Although we did not observe other developmental or phototransduction defects in cones with mislocalized nuclei, their dark adaptation was impaired, consistent with a deficiency in chromophore recycling. These findings demonstrate that the apical localization of cone nuclei in the ONL is required for the timely dark adaptation and efficient synaptic transmission in cone photoreceptors.

Keywords

cone photoreceptor; dark adaptation; retina electrophysiology; nucleus migration; LINC complex; retinal degeneration

Introduction

Ciliary photoreceptors are the primary light-sensing cells that initiate vision in vertebrates. There are two types of vertebrate ciliary photoreceptors, rods and cones, which have distinct morphological and functional properties. Rods are very sensitive to light but become saturated at daylight conditions, while cones do not saturate in bright light, and mediate daylight vision (1–3). The nuclei of rods and cones form the outer nuclear layer (ONL) of the retina. Intriguingly, in rod-dominant retinas, such as mouse and human, the cone nuclei

Corresponding author: Yunlu Xue, PhD, Department of Genetics, Harvard Medical School, Boston, MA 02115;, Tel: (617) 432-6531;, Fax: (617) 432-7595; yunlu_xue@hms.harvard.edu.

Author Contributions

V.K., D.H., and Y.X. designed research; Y.X. and D.R. performed research and analyzed data; Y.X., V.K., and D.H. wrote the paper.

locate specifically at the apical (i.e. outer) side of the ONL. Thus cone nuclei are adjacent to the inner segments of the cones, which is a cellular structure enriched in organelles, most notably mitochondria (4). Rod nuclei comprise the remainder of the ONL, exclusively populating the basal (i.e. inner) side of the ONL, which is adjacent to the outer plexiform layer (OPL), composed of synaptic terminals.

This arrangement of cone and rod nuclei is evolutionarily conserved, e.g. it has been observed in the lamprey "long" photoreceptors, the analog of cones (5–7). In cone-dominant retinas such as in zebrafish (8), chicken (9), and ground squirrel (10), cone nuclei also preferentially localize apically within the ONL. Even in the fovea, which is populated exclusively by cones, cone nuclei seem to be distanced from their synaptic terminals by inner photoreceptor fibre layer in birds (11), or by Henle Fiber Layer in primates (12), Overall, there is a marked preference for cones to localize their nuclei adjacent to their inner segments and distal to their synaptic terminals. This arrangement is even more unusual considering that cone precursor nuclei actively migrate across the entire ONL during retinal development, before settling into their final position at the apical side of the ONL, around postnatal day P11 in the case of mice (13, 14).

The reason why cone nuclei localization is biased toward the apical side of the ONL is unknown, and whether such precise nuclear positioning is required for normal cone-mediated vision remains to be determined. We have previously shown that Linkers of the Nucleoskeleton to the Cytoskeleton (LINC complexes) are essential for the migration of cone nuclei in the mouse retina (14, 15). LINC complexes are macromolecular assemblies of the nuclear envelope, and formed through the interaction of Sun proteins and Nesprins across the nuclear envelope (16). This interaction is mediated by the evolutionarily conserved KASH (Klarsicht/Anc-1/Syne1 homology) domain of Nesprins and the SUN domain of Sun proteins. Using an in vivo dominant-negative strategy targeting the KASH domain of Nesprins (17, 18), we were able to disrupt nuclear migration, and mislocalize a fraction of the cone nuclei to the basal side of the ONL (14). This approach provides a unique way of investigating the role of cone nuclear localization. We opted for this strategy over alternative genetic approaches for disrupting the LINC complex, because of Nesprin isoform diversity (19), and the premature death of Sun1/2 double knockouts upon birth (20).

In this study, we used a new line of dominant-negative KASH mice that efficiently and specifically affect the nuclear positioning in cone photoreceptors (21). In this mouse line, the vast majority of cone nuclei mislocalize to the basal side of the ONL. This setting allowed us to investigate the possible structural and functional roles of the localization of cone nuclei at the apical side of the ONL.

Materials and Methods

Animals

Mice used for the study were 12–14 weeks old littermates, derived from crossing *Gnat1*$^{-/-}$ line (transducin α-subunit knockout) with Tg(CAG-LacZ/EGFP-KASH2) and/or Tg(HRGP-*Cre*) lines described previously (21–23). The cone nuclei mislocalization mice are referred to as ^{HRGP}EGFP-KASH2. Only cones, but not rods, are able to respond to light in these

animals, allowing for careful quantitative analysis of cone function. All animals were free of *rd8* mutation (24). The maintenance and treatment of the animals followed the protocols approved by Washington University Animal Studies Committee.

Electron microscopy

Eyecups were fixed for 12–24 h by immersion in 2% paraformaldehyde plus 3% glutaraldehyde in 0.1 M sodium phosphate buffer (pH 7.35), post-fixed in 1% osmium tetroxide for 1 h, and stained en bloc with 1% uranyl acetate in 0.1 M acetate buffer for 1 h. Blocks were then dehydrated in a graded series of ethanol incubations, followed by propylene oxide. They were then embedded in Araldite 6005 resin. Sagittal semi-thin sections of the entire retina were taken at the level of the optic nerve, and a ~700 μm^2 area just lateral to the optic nerve was blocked for further analysis. Ultrathin sections were cut on a Leica Ultracut R microtome, mounted on formvar-coated slot grids, and post-stained with uranyl acetate and lead citrate. The tissue was examined with a Hitachi −7500 electron microscope, and images were recorded with a digital camera.

Immunohistochemistry imaging

Cryosections (15 μm) on Millennia 1000 slides (StatLab) were fixed for 5 min in 4% PFA in PBS, rinsed three times in PBS, permeabilized in 0.5% Triton-X100/PBS, and incubated with primary antibodies diluted in 10% donkey serum/0.5% Triton X-100 in PBS. Secondary antibodies conjugated to Alexa 594, 488 or 647 (Invitrogen) were incubated in the same conditions. Following DAPI staining, slices were mounted in fluorescent mounting medium (DAKO). Cone arrestin (Millipore) antibody was used in this study. A Nikon Eclipse Ti fluorescence microscope, which was coupled to an LED light source (Lumencor), was used to image the sections with either 20X (n.a. 1.0) or 40X (n.a. 1.4) objectives. The NIS element software package (Nikon) was used for the image acquisition and analysis. The number of cones was counted with the quantification tools from NIS-Elements (Nikon). Cones labelled with specific markers were counted in at least two fields from at least two central retina slices crossing the optic nerve without tracking the orientation of retina. The total number of cones was divided by the length of a reference line drawn on the apical row of the ONL.

Electroretinography (ERG)

In vivo electroretinogram (ERG) recordings were done with a commercially available LKC® ERG system as described previously (25–27). All mice were dark-adapted for at least 18 hours before the experiment. The dark-adapted animals were anesthetized with ketamine-xylazine cocktail (100/20 mg/kg) and their pupils were dilated with atropine eye-drops. A mouse was placed on a heating pad (37 °C), and contact-lens electrodes were placed on both eyes for recording the retinal signals. The animal was allowed to stabilize for 15 minutes in darkness before the beginning of the recordings. For dark-adapted ERG tests on these *Gnat1*$^{-/-}$ mice, multiple responses were elicited at different flash intensities from 0.0227 to 697 cd s/m^2, and the averaged cone b-wave amplitude was measured. The oscillatory potentials at 23.5 cd s/m^2 were isolated through a 0.1 Hz high-pass filter. Prior to the bleach, the maximal response and dim flash response were recorded using 697 and 0.238 cd s/m^2 flash intensities, respectively. A 30 seconds bright light was applied to both eyes to

photobleach an estimated 90% of the cone visual pigment with a custom-made green LED light source (25). The recovery of sensitivity was measured at fixed time intervals after the bleach, and normalized to the pre-bleach level.

Transretinal recording

This technique was described in detail previously (28, 29). Briefly, mice were dark adapted overnight before euthanasia by CO_2. The eyes were immediately excised and dissected under infrared light-fitted microscope. The whole retina was carefully removed from the eye cup, and mounted to a recording chamber with the photoreceptor side facing the light source. The retina was perfused by 95% O_2/ 5% CO_2 bubbled Locke's solution containing 30 μM DL-AP4 to inhibit synaptic transmission and block the b-wave. Before the recordings, the retina was allowed to stabilize for 15 minutes in darkness. A 505 nm LED light source was used to induce cone photoresponses. The duration and intensity of light pulse were controlled by computer-run pClamp9 software (Molecular Devices). The transretinal voltage changes induced by the test flash were amplified, digitized, and recorded in the computer. After recording a series of dark-adapted responses to increasing light intensities, the retina was exposed to 3 seconds of bright light, estimated to bleach 90% of the visual pigment. The subsequent recovery of sensitivity was recorded using a pre-programmed protocol, and normalized to its pre-bleach level (25, 26, 30).

Statistical Analysis

One-way ANOVA and Student's t-test (two-way, unpaired) was used to determine the statistical significance of measured parameters for all the data shown in this study.

Results

EGFP-KASH2 is a fusion protein of the KASH domain of Nesprin2 and EGFP. In cultured cells, it localizes at the nuclear envelope where it displays typical fluorescent nuclear rims. Importantly, EGFP-KASH2 acts in a dominant-negative manner on endogenous SUN/KASH interactions by displacing Nesprins from the outer nuclear membrane (ONM) to the endoplasmic reticulum, and in effect, it leads to the disruption of the endogenous LINC complexes (31–33). In mice, the conditional transgenic expression of EGFP-KASH2 prevents the apical migration of developing cone photoreceptor nuclei during postnatal retinal development (14). However, the mosaic expression pattern of EGFP-KASH2 in these animals prevented the functional assessment of nuclear mislocalization in adult cones. For this reason, we replaced the CMV promoter of our original conditional transgenic construct with the CAG promoter (Figure 1A) that significantly improved expression (34). In these mice, EGFP-KASH2 is robustly expressed in a wider array of tissues (21, 35).

Transgenic expression of EGFP-KASH2 was targeted to differentiating cone photoreceptors by breeding Tg(CAG-LacZ/EGFP-KASH2) mice with Tg(HRGP-Cre) mice, which initiate cone-specific expression of Cre recombinase at P6 (36) (Figure 1A). As expected, EGFP-KASH2 was specifically expressed in more than 90% of the cones within adult recombinant retinas (called ^{HRGP}EGFP-KASH2 hereafter), as GFP+ rims were exclusively observed around cone arrestin (CAR) positive nuclei (Figure 1B; bottom). The cone nuclei surrounded

by the EGFP-KASH2+ rim accumulated in the basal ONL and the outer plexiform layer (OPL) of ^{HRGP}EGFP-KASH2 retina (Figure 1B; bottom). In contrast, HRGP-Cre control cone nuclei were located on the apical ONL beneath the inner and outer segments (IS and OS) (Figure 1B; top). In agreement with light microscopy data, electron microscopy revealed that the OPL of ^{HRGP}EGFP-KASH2 retinas were populated with cone nuclei in close proximity to the cone pedicles, whereas the OPL of HRGP-Cre control retinas were free of cone nuclei and displayed typical cone pedicles (Figure 1C; bottom). Despite the morphological change of cone pedicles, synaptic ribbons and synaptic densities were detected in both ^{HRGP}EGFP-KASH2 and HRGP-Cre cones. In addition, we did not detect any obvious morphological defects of either the IS or OS of cone photoreceptors (Figure 1C; top). Finally, there were no significant differences in the number of cones in ^{HRGP}EGFP-KASH2 and HRGP-Cre central retinas at P25 and P120, however, at P450, ^{HRGP}EGFP-KASH2 central retinas displayed a significant loss of cone numbers compared to controls (Figure 1D). Together, these results indicate that the mislocalization of ^{HRGP}EGFP-KASH2 cone nuclei profoundly alters the structural organization of cone pedicles, but without affecting IS/OS development, and eventually leads to cone death.

To determine the functional consequences of cone nuclei mislocalization, we first crossed ^{HRGP}EGFP-KASH2 mice to *Gnat1*$^{-/-}$ background to eliminate the photoresponse of rods, thus facilitating the physiological recordings of pure cone signals (23, 25). We then used *in vivo* ERG recordings to assess the cone-driven responses of ^{HRGP}EGFP-KASH2 mutant and control HRGP-Cre mice to light stimuli at an early age before the onset of cone degeneration (Figure 2A). The most prominent alteration was a ~37% reduction in the amplitude of cone b-wave ERG responses (Figure 2C). The cone b-wave sensitivity (as measured from the half-saturating test flash intensity, $I^{b}_{1/2}$) of mutant mice remained largely unchanged, even though their normalized responses to dim flashes were significantly smaller than the corresponding responses of the control mice (Figure 2D). This result suggests a possible alteration in the efficiency of synaptic transmission between cones and cone bipolar cells that effectively reduced the dynamic range of the signal transmitted downstream to the inner retina. In addition, the oscillatory potentials (OP) of the ^{HRGP}EGFP-KASH2 mutant mice were severely decreased in amplitude, and the timing of OP was also delayed compared to controls (Figure 2B). The origin of the OP within the retina is still a subject of debate (37), but the OP phenotype observed in ^{HRGP}EGFP-KASH2 mice could, at least in part, be explained by the decrease in their b-wave amplitude.

The ERG b-wave is not a direct measurement of cone function, because it measures the ON-bipolar cell activity that is driven by the synaptic signaling from the cones. The ERG a-wave assays the photoresponse of cones, but the mouse cone a-wave is too small and difficult to quantify *in vivo*. Thus, to further investigate if the observed cone b-wave amplitude reduction was caused by alteration in phototransduction or by suppressing synaptic transmission, we used transretinal recordings to directly assess the function of these cones *ex vivo*. In transretinal recording, we could isolate the cone a-wave by adding synaptic transmission inhibitors in the perfusion solution to block the b-wave (38) (Figure 3A). We found that the kinetics of dim flash photoresponses showed no difference in mutant cones compared to the HRGP-Cre control cones (Figure 3B). Thus, the rates of activation and inactivation of the phototransduction cascade were not affected by the mislocalization of

cone nuclei. In addition, in contrast to the reduced b-wave amplitude of *HRGP*EGFP-KASH2 mice, the maximal response of their cone response was comparable to that of the control HRGP-Cre control cones (Figure 3C). Taken together, these results suggested that the cone b-wave amplitude reduction was caused not by changes in cone phototransduction, but rather by altered cone synaptic transmission. This finding is consistent with the normal morphology of cone inner and outer segments, as well as the disruption of synaptic pedicles in *HRGP*EGFP-KASH2 cones (Figure 1B and C).

Notably, we observed that the a-wave sensitivity ($I^a_{1/2}$) of the mutant cones was slightly decreased by 2.5-fold (Figure 3D). However, this desensitization was compensated in downstream (e.g. by synaptic transmission and/or bipolar cell transduction), resulting in an unaffected $I^b_{1/2}$ (Figure 2D). This slight drop in $I^a_{1/2}$ was unlikely due to a change in phototransduction amplification as the dim flash kinetics were normal (Figure 3B). However, this result was reminiscent of our previous study on a strain of visual cycle deficient mice, which also had desensitized cones due to a suppressed chromophore recycling for cone opsin regeneration (26). Thus, we next measured the kinetics of cone dark adaptation in mutant and control mice following exposure to bright light that would rapidly bleach most of the visual pigment in the cones. The subsequent recovery (i.e. dark adaptation) is driven by the regeneration of the bleached cone visual pigment, which, in turn, is rate-limited by the recycling of visual chromophore (39, 40).

First, we found that the cone b-wave sensitivity (S_f/S_f^{DA}) recovery was 2.6-fold lower in *HRGP*EGFP-KASH2 mice compared to controls at 50 minutes after bleach (Figure 4A). As the late phase of cone dark adaptation is driven by the retina pigment epithelium (RPE) visual cycle in normal conditions (25), this finding might indicate that the mislocalization of cone nuclei in the *HRGP*EGFP-KASH2 mice impairs the recycling of chromophore between cones and the RPE. Second, we found that the initial phase of cone recovery, driven by the retina visual cycle through Müller glial cells in normal conditions (25, 40), was also suppressed in the *HRGP*EGFP-KASH2 eyes (Figure 4A). To directly examine the Müller glial cell visual cycle efficiency, we measured cone dark adaptation in isolated retinas using transretinal recordings. In these conditions, cone pigment regeneration is driven exclusively by the retina visual cycle through the Müller glial cells (41). We found that the level of cone sensitivity recovery in the isolated *HRGP*EGFP-KASH2 retinas was reduced by 1.5-fold compared to the control at 7 minutes after bleach (Figure 4B). Thus, the supply of chromophore to cones from Müller glial cells also appeared to be compromised in the retinas of *HRGP*EGFP-KASH2 mice.

Discussion

It is well established that the nuclei of cone photoreceptors localize exclusively to the apical side of the outer nuclear layer within the vertebrate retina. This specific localization of cone nuclei is highly evolutionarily conserved and can be found in the retinas of both rod- and cone-dominant species. Our results suggest that cone nuclei positioning at the apical side of ONL is important for maintaining proper cone pedicle morphology. The observed normal cone-driven responses but reduced bipolar cell-driven responses also suggest that cone nuclear position could be required for proper synaptic transmission from cones to their

bipolar cell partners. The greatly suppressed oscillatory potentials that we observed in *HRGP*EGFP-KASH2 mice also support this notion. Future direct recordings from cone bipolar cells will be needed to confirm this notion. The mispositioning of cone nuclei also directly causes moderate reduction of cone sensitivity, consistent with alterations in the visual cycle as reflected by the impaired cone dark adaptation. One possible cause of the cone loss in older mice (Figure 1D) could be the chronic chromophore deficiency caused by a possible deteriorated visual cycle, as has been observed in other visual cycle deficient animals (26, 42, 43).

The mechanism(s), by which the mislocalization of cone nuclei results in a possible suppressed recycling of cone chromophore by the RPE/Müller glial cells, is currently unknown. One possibility is that cone nuclei might serve as a “pool” for the hydrophobic retinoid chromophore. Another possibility is that the apical presence of cone nuclei increases the surface area of the plasma membrane, thus enhances the efficiency of the retinoid exchange between cones and RPE/Müller glial cells. Alternatively, cone nuclei could physically anchor certain unidentified cone-specific visual cycle enzyme(s) (30, 44). In any case, placing the cone nucleus too far away from the inner and outer segments might restrict chromophore recycling and supply to the outer segment, where cone pigment regeneration takes place.

In summary, our results indicate that the normal positioning of cone nuclei is important for maintaining normal cone function, including cone sensitivity, cone-to-bipolar-cell signal transmission, and cone visual pigment regeneration.

Acknowledgments

This work was funded by the National Eye Institute (EY025696 and EY027387 to V.J.K., EY022632 to D.H., and K99EY030951 to Y.X.), a National Eye Institute Center Core Grant (P30EY002687) and an unrestricted grant to the Washington University Department of Ophthalmology and Visual Sciences from Research to Prevent Blindness. We thank Belinda McMahan and Frank Schottler from the Morphology and Imaging Core of the Department of Ophthalmology and Visual Sciences for their technical support, and the team at the Mouse Genetics Core for handling mice breeding and genotyping. The authors are grateful to Dr. Yun-Zheng Le (University of Oklahoma Health Sciences Center) for sharing the HRGP-*Cre* strain, and to Dr. Janis Lem (Tufts University) for the *Gnat1*$^{-/-}$ strain. We also thank Dr. Connie Cepko at Harvard Medical School for insightful comments and constructive feedbacks on this project and manuscript.

Nonstandard Abbreviations

LINC	Linkers of the Nucleoskeleton to the Cytoskeleton
KASH	Klarsicht/Anc-1/Syne1 homology
ERG	electroretinography
OP	oscillatory potentials
INM	inner nuclear membrane
ONM	outer nuclear membrane
CAR	cone arrestin

OS	outer segments
IS	inner segments
ONL	outer nuclear layer
OPL	outer plexiform layer
CP	cone pedicle
RS	rod spherule
CN	cone nucleus
RN	rod nucleus

References

1. Yau KW and Hardie RC (2009) Phototransduction motifs and variations. Cell 139, 246–264 [PubMed: 19837030]
2. Lamb TD, Collin SP, and Pugh EN (2007) Evolution of the vertebrate eye: opsins, photoreceptors, retina and eye cup. Nat. Rev. Neurosci 8, 960–976 [PubMed: 18026166]
3. Fain GL, Hardie R, and Laughlin SB (2010) Phototransduction and the evolution of photoreceptors. Curr. Biol 20, R114–24 [PubMed: 20144772]
4. Hoang Q, Linsenmeier R, Chung C, and Curcio C (2002) Photoreceptor inner segments in monkey and human retina: mitochondrial density, optics, and regional variation. Vis. Neurosci 19, 395–407 [PubMed: 12511073]
5. Dickson DH and Graves DA (1979) Fine structure of the lamprey photoreceptors and retinal pigment epithelium (Petromyzon marinus L.). Exp. Eye Res 29, 45–60 [PubMed: 228957]
6. Ishikawa M, Takao M, Washioka H, Tokunaga F, Watanabe H, and Tonosaki A (1987) Demonstration of rod and cone photoreceptors in the lamprey retina by freeze-replication and immunofluorescence. Cell Tissue Res. 249, 241–246 [PubMed: 3304647]
7. Morshedian A and Fain GL (2015) Single-photon sensitivity of lamprey rods with cone-like outer segments. Curr. Biol 25, 484–487 [PubMed: 25660538]
8. Lagman D, Callado-Pérez A, Franzén IE, Larhammar D, and Abalo XM (2015) Transducin duplicates in the zebrafish retina and pineal complex: differential specialisation after the teleost tetraploidisation. PLoS One 10, e0121330 [PubMed: 25806532]
9. López-López R, López-Gallardo M, Pérez-Alvarez MJ, and Prada C (2008) Isolation of chick retina cones and study of their diversity based on oil droplet colour and nucleus position. Cell Tissue Res. 332, 13–24 [PubMed: 18266011]
10. Cuenca N, Deng P, Linberg KA, Lewis GP, Fisher SK, and Kolb H (2002) The neurons of the ground squirrel retina as revealed by immunostains for calcium binding proteins and neurotransmitters. J. Neurocytol 31, 649–666 [PubMed: 14501205]
11. Bringmann A (2019) Structure and function of the bird fovea. Anat. Histol. Embryol 48, 177–200 [PubMed: 30734347]
12. Kolb H (2011) WEBVISION - Simple Anatomy of the Retina.
13. Rich KA, Zhan Y, and Blanks JC (1997) Migration and synaptogenesis of cone photoreceptors in the developing mouse retina. J. Comp. Neurol 388, 47–63 [PubMed: 9364238]
14. Razafsky D, Blecher N, Markov A, Stewart-Hutchinson PJ, and Hodzic D (2012) LINC Complexes Mediate the Positioning of Cone Photoreceptor Nuclei in Mouse Retina. PLoS One 7, e47180 [PubMed: 23071752]
15. Razafsky D, Wirtz D, and Hodzic D (2014) Nuclear Envelope in Nuclear Positioning and Cell Migration. In Advances in experimental medicine and biology vol. 773, pp. 471–490, [PubMed: 24563361]

16. Crisp M, Liu Q, Roux K, Rattner JB, Shanahan C, Burke B, Stahl PD, and Hodzic D (2006) Coupling of the nucleus and cytoplasm: role of the LINC complex. J. Cell Biol 172, 41–53 [PubMed: 16380439]
17. Sosa BA, Rothballer A, Kutay U, and Schwartz TU (2012) LINC complexes form by binding of three KASH peptides to domain interfaces of trimeric SUN proteins. Cell 149, 1035–1047 [PubMed: 22632968]
18. Zhou Z, Du X, Cai Z, Song X, Zhang H, Mizuno T, Suzuki E, Yee MR, Berezov A, Murali R, Wu S-L, Karger BL, Greene MI, and Wang Q (2012) Structure of Sad1-UNC84 homology (SUN) domain defines features of molecular bridge in nuclear envelope. J. Biol. Chem 287, 5317–5326 [PubMed: 22170055]
19. Rajgor D and Shanahan CM (2013) Nesprins: from the nuclear envelope and beyond. *Expert Rev.* Mol. Med 15, e5
20. Lei K, Zhang X, Ding X, Guo X, Chen M, Zhu B, Xu T, Zhuang Y, Xu R, and Han M (2009) SUN1 and SUN2 play critical but partially redundant roles in anchoring nuclei in skeletal muscle cells in mice. Proc. Natl. Acad. Sci. U. S. A 106, 10207–10212 [PubMed: 19509342]
21. Razafsky D and Hodzic D (2014) Temporal and tissue-specific disruption of LINC complexes in vivo. genesis 52, 359–365 [PubMed: 24550182]
22. Yang SH, Chang SY, Yin L, Tu Y, Hu Y, Yoshinaga Y, de Jong PJ, Fong LG, and Young SG (2011) An absence of both lamin B1 and lamin B2 in keratinocytes has no effect on cell proliferation or the development of skin and hair. Hum. Mol. Genet 20, 3537–3544 [PubMed: 21659336]
23. Calvert PD, Krasnoperova NV, Lyubarsky a L., Isayama T, Nicoló M, Kosaras B, Wong G, Gannon KS, Margolskee RF, Sidman RL, Pugh EN, Makino CL, and Lem J (2000) Phototransduction in transgenic mice after targeted deletion of the rod transducin alpha -subunit. Proc. Natl. Acad. Sci. U. S. A 97, 13913–13918 [PubMed: 11095744]
24. Mattapallil MJ, Wawrousek EF, Chan C-C, Zhao H, Roychoudhury J, Ferguson TA, and Caspi RR (2012) The Rd8 mutation of the Crb1 gene is present in vendor lines of C57BL/6N mice and embryonic stem cells, and confounds ocular induced mutant phenotypes. Invest. Ophthalmol. Vis. Sci 53, 2921–2927 [PubMed: 22447858]
25. Kolesnikov AV, Tang PH, Parker RO, Crouch RK, and Kefalov VJ (2011) The Mammalian cone visual cycle promotes rapid m/l-cone pigment regeneration independently of the interphotoreceptor retinoid-binding protein. 2. J. Neurosci 31, 7900–7909 [PubMed: 21613504]
26. Xue Y, Shen SQ, Jui J, Rupp AC, Byrne LC, Hattar S, Flannery JG, Corbo JC, and Kefalov VJ (2015) CRALBP supports the mammalian retinal visual cycle and cone vision. J. Clin. Invest 125, 727–738 [PubMed: 25607845]
27. Xue Y, Shen SQ, Corbo JC, and Kefalov VJ (2015) Circadian and light-driven regulation of rod dark adaptation. Sci. Rep 5, 17616 [PubMed: 26626567]
28. Vinberg F, Kolesnikov AV, and Kefalov VJ (2014) Ex vivo ERG analysis of photoreceptors using an in vivo ERG system. Vision Res. 101, 108–117 [PubMed: 24959652]
29. Kolesnikov AV and Kefalov VJ (2012) Transretinal ERG recordings from mouse retina: rod and cone photoresponses. J. Vis. Exp
30. Xue Y, Sato S, Razafsky D, Sahu B, Shen SQ, Potter C, Sandell LL, Corbo JC, Palczewski K, Maeda A, Hodzic D, and Kefalov VJ (2017) The role of retinol dehydrogenase 10 in the cone visual cycle. Sci. Rep 7, 2390 [PubMed: 28539612]
31. Stewart-Hutchinson PJ, Hale CM, Wirtz D, and Hodzic D (2008) Structural requirements for the assembly of LINC complexes and their function in cellular mechanical stiffness. Exp. Cell Res 314, 1892–1905 [PubMed: 18396275]
32. Roux KJ, Crisp ML, Liu Q, Kim D, Kozlov S, Stewart CL, and Burke B (2009) Nesprin 4 is an outer nuclear membrane protein that can induce kinesin-mediated cell polarization. Proc. Natl. Acad. Sci. U. S. A 106, 2194–2199 [PubMed: 19164528]
33. Lombardi ML, Zwerger M, and Lammerding J (2011) Biophysical assays to probe the mechanical properties of the interphase cell nucleus: substrate strain application and microneedle manipulation. J. Vis. Exp

34. Alexopoulou AN, Couchman JR, and Whiteford JR (2008) The CMV early enhancer/chicken beta actin (CAG) promoter can be used to drive transgene expression during the differentiation of murine embryonic stem cells into vascular progenitors. BMC Cell Biol. 9, 2 [PubMed: 18190688]

35. Razafsky D, Potter C, and Hodzic D (2015) Validation of a Mouse Model to Disrupt LINC Complexes in a Cell-specific Manner. J. Vis. Exp

36. Le Y, Zheng L, Zheng W, Ash JD, Agbaga M, Zhu M, and E R (2006) Technical Brief Mouse opsin promoter-directed Cre recombinase expression in transgenic mice. Mol. Vis

37. Wachtmeister L (1998) Oscillatory potentials in the retina: what do they reveal. Prog. Retin. Eye Res 17, 485–521 [PubMed: 9777648]

38. Stockton RA and Slaughter MM (1989) B-wave of the electroretinogram. A reflection of ON bipolar cell activity. J. Gen. Physiol 93, 101–122 [PubMed: 2915211]

39. Lamb TD and Pugh EN (2004) Dark adaptation and the retinoid cycle of vision. Prog. Retin. Eye Res 23, 307–380 [PubMed: 15177205]

40. Wang J, Nymark S, Frederiksen R, Estevez ME, Shen SQ, Corbo JC, Cornwall MC, and Kefalov VJ (2014) Chromophore supply rate-limits mammalian photoreceptor dark adaptation. J. Neurosci 34, 11212–11221 [PubMed: 25143602]

41. Wang JS, Estevez ME, Cornwall MC, and Kefalov VJ (2009) Intra-retinal visual cycle required for rapid and complete cone dark adaptation. Nat. Neurosci 12, 295–302 [PubMed: 19182795]

42. Redmond TM, Yu S, Lee E, Bok D, Hamasaki D, Chen N, Goletz P, Ma JX, Crouch RK, and Pfeifer K (1998) Rpe65 is necessary for production of 11-cis-vitamin A in the retinal visual cycle. Nat. Genet 20, 344–351 [PubMed: 9843205]

43. Zhang H, Fan J, Li S, Karan S, Rohrer B, Palczewski K, Frederick JM, Crouch RK, and Baehr W (2008) Trafficking of membrane-associated proteins to cone photoreceptor outer segments requires the chromophore 11-cis-retinal. J. Neurosci 28, 4008–4014 [PubMed: 18400900]

44. Sato S, Frederiksen R, Cornwall MC, and Kefalov VJ (2017) The retina visual cycle is driven by cis retinol oxidation in the outer segments of cones. Vis. Neurosci 34, E004 [PubMed: 28359344]

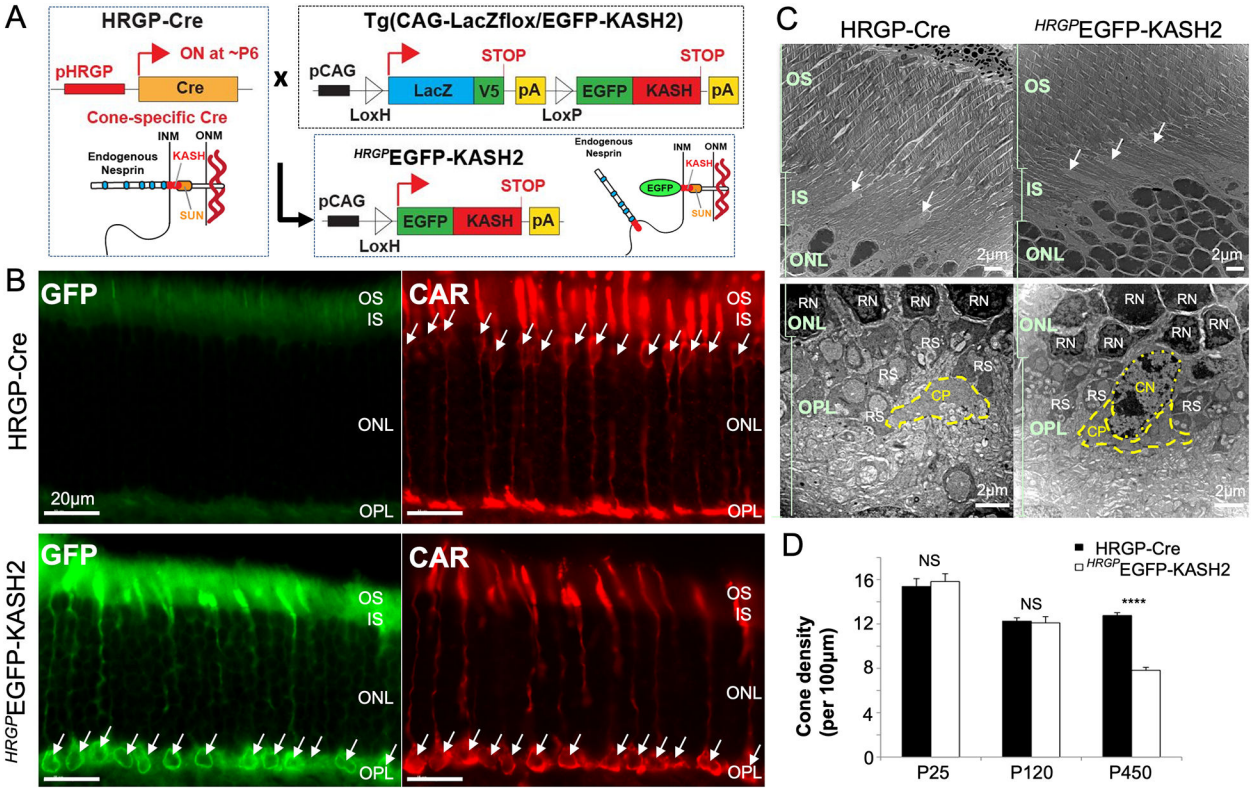

Figure 1.

Expression of ^{HRGP}EGFP-KASH2 in cones. **(A)** The genetic modification strategy used to create ^{HRGP}EGFP-KASH2 cones. **(B)** Fluorescence images of HRGP-Cre cones and ^{HRGP}EGFP-KASH2 cones at P55, labeled by GFP and cone arrestin. *Arrows*: the location of individual cone nuclei in normal (top) and mislocalized (bottom) position. *Scale bar*: 20μm. **(C)** Transmission electron microscopic (TEM) images of the inner and outer segments (top) cone pedicles (bottom) in P25 HRGP-*Cre* control and ^{HRGP}EGFP-KASH2 retinas. *Arrows*: cone inner segments. *Dash lines*: the boundary of cone pedicles and a mislocalized cone nucleus. *Scale bar*: 2μm. **(D)** Central cone densities estimated by counting CAR+ cells using >3 fields of both retinas from 2 distinct animals per genotype and time point. *Abbreviations*: inner nuclear membrane (INM), outer nuclear membrane (ONM), cone arrestin (CAR), outer segments (OS) and inner segments (IS) of photoreceptors, outer nuclear layer (ONL), and outer plexiform layer (OPL), cone pedicle (CP), rod spherule (RS), cone nucleus (CN), and rod nucleus (RN). All data are presented as mean ± SEM. ****P << 0.0001; NS, not significant i.e. P > 0.05.

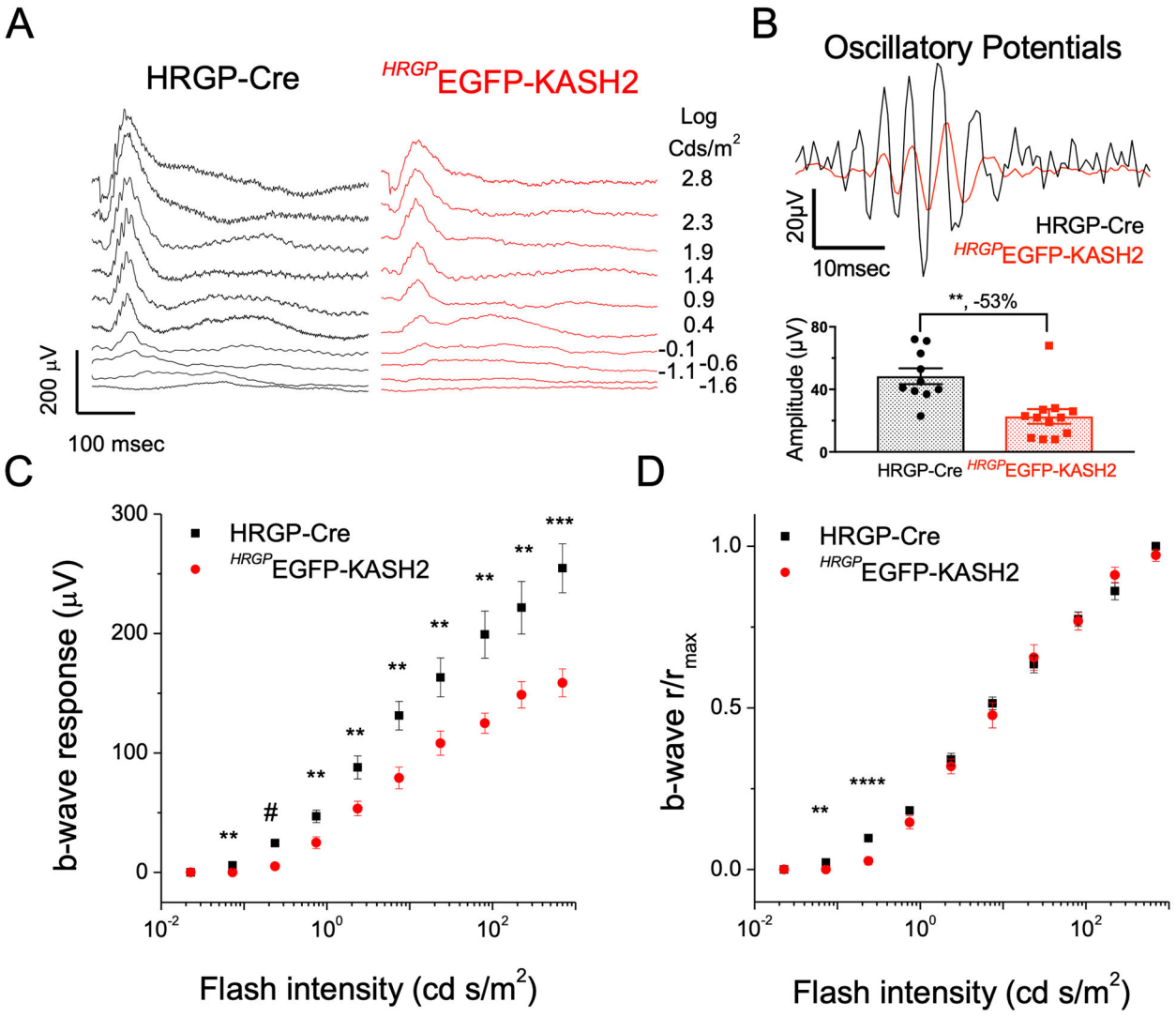

Figure 2.

Effect of ^{HRGP}EGFP-KASH2 on cone-driven responses from *in vivo* ERG recordings. **(A)** Representative ERG response families from HRGP-Cre *Gnat1*$^{-/-}$ (control), and ^{HRGP}EGFP-KASH2 *Gnat1*$^{-/-}$ (mutant) eyes. **(B)** Representative (upper panel), and amplitude-averaged (lower panel) data of ERG oscillatory potentials from control and mutant eyes. *Flash intensity*: 23.5 cd s/m^2. **(C)** Averaged dark-adapted cone b-wave intensity response curves, and **(D)** the normalized dark-adapted cone b-wave intensity response curves, of control (n=10) and mutant (n=12) mice. All data are presented as mean ± SEM. **P < 0.01, ***P < 0.001, ****P < 0.0001, #P < 1 × 10^{-5}.

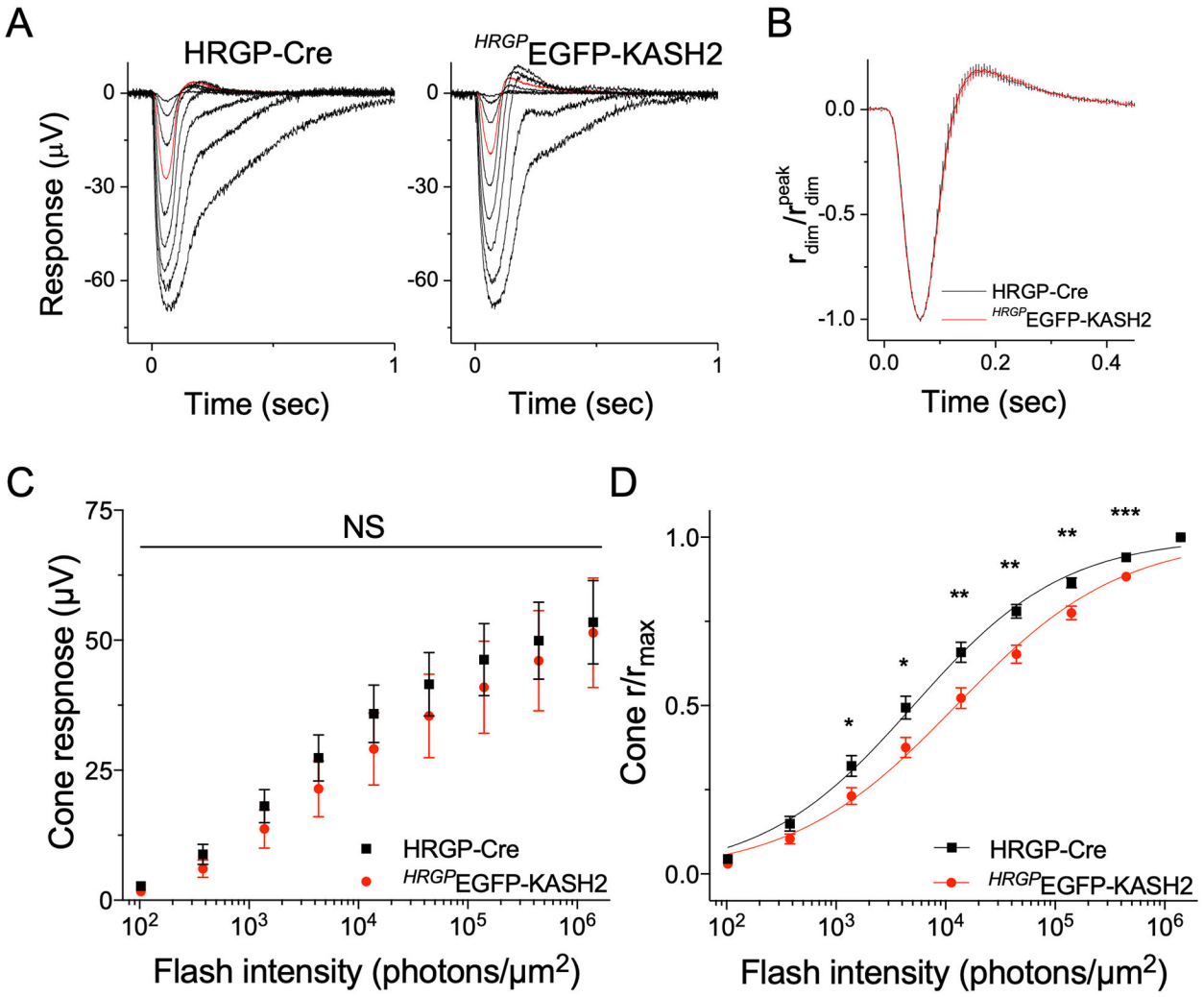

Figure 3.

Effect of ^{HRGPE}EGFP-KASH2 on cone responses from *ex vivo* transretinal recordings. **(A)** Representative transretinal response families from HRGP-Cre *Gnat1*$^{-/-}$ (control) and ^{HRGP}EGFP-KASH2 *Gnat1*$^{-/-}$ (mutant) retinas (red trace flash intensity: 4,320 photons/μm^2). **(B)** Averaged normalized dim flash responses of control (n=10) and mutant (n=10) retinas. **(C)** The intensity response curve, and **(D)** the normalized intensity response curve, of control (n=12) and mutant (n=14) retinas. The Hill Function fitting curves: $R = I^{0.63}/(I^{0.63} + 5{,}081^{0.63})$ for the control, and $R = I^{0.58}/(I^{0.58} + 12{,}474^{0.58})$ for the mutant. All data are presented as mean ± SEM. *P < 0.05, **P < 0.01, ***P < 0.001; NS, not significant i.e. P > 0.05.

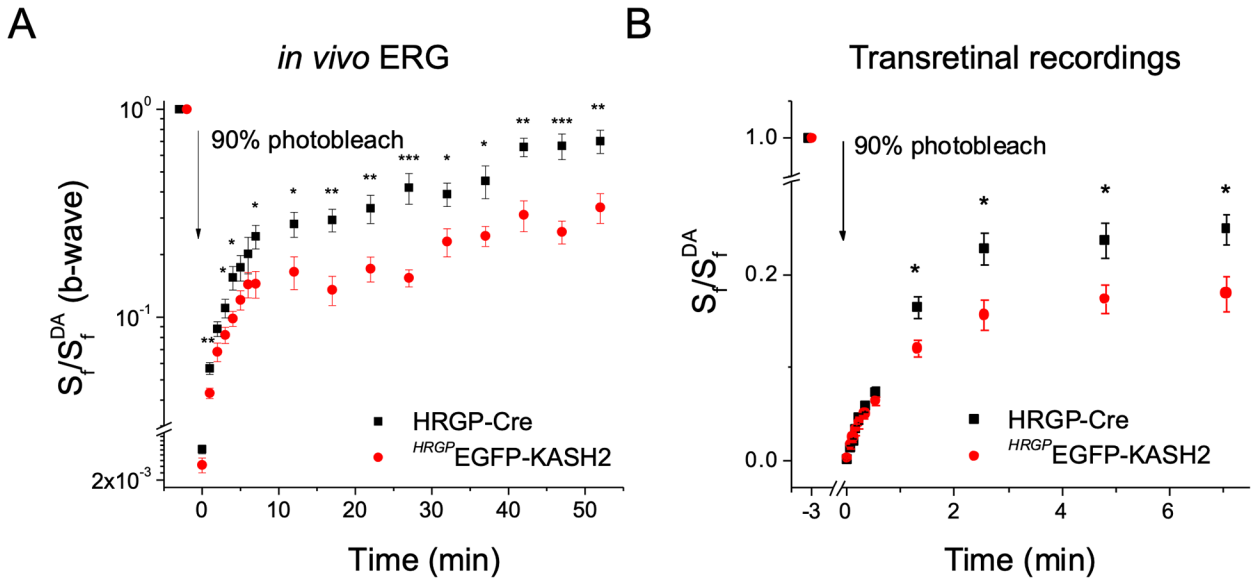

Figure 4.

The recovery kinetics of cone sensitivity following 90% photobleach on *Gnat1*$^{-/-}$ background. **(A)** The cone b-wave sensitivity recovery measured through *in vivo* ERG recordings. The cone recovery is driven by both of the Müller glial cell visual cycle (initial fast phase) and the RPE visual cycle (later slower phase). The pre-bleach b-wave sensitivity, S_f^{DA}, was 104 ± 11 μV*m^2/cd s for control (n=8) and 88 ± 3 μV*m^2/cd s for mutant (n=10) eyes, NS. **(B)** The cone sensitivity recovery measured through *ex vivo* transretinal recordings. The cone recovery in this case is driven only by the Müller glial cell visual cycle. S_f^{DA} was 0.015 ± 0.002 μV*μm^2/ph for control (n=9) and 0.011 ± 0.002 μV*μm^2/ph for mutant (n=7) retinas, NS. All data are presented as mean ± SEM. *P < 0.05, **P < 0.01, ***P < 0.001; NS, not significant i.e. P > 0.05.